Equation of State and Collective Dynamics

Ulrich Heinz[1]

Department of Physics, The Ohio State Univesity, Columbus, OH 43210, USA

Abstract. This talk summarizes the present status of a program to quantitatively relate data from the Relativistic Heavy Ion Collider (RHIC) on collective expansion flow to the Equation of State (EOS) of hot and dense strongly interacting matter, including the quark-gluon plasma and the quark-hadron phase transition. The limits reached with the present state of the art and the next steps required to make further progress will both be discussed.

1. The QCD Equation of State and ideal fluid dynamics

With relativistic heavy-ion collisions one explores the phase diagram of strongly interacting bulk matter in the regime of high energy density and temperature. Lattice QCD (LQCD) tells us [1] that for zero net baryon density QCD matter undergoes a phase transition at $T_{\rm cr} = 173 \pm 15\,{\rm MeV}$ from a color-confined hadron resonance gas (HG) to a color-deconfined quark-gluon plasma (QGP). The critical energy density $e_{\rm cr} \simeq 0.7\,{\rm GeV/fm}^3$ [1] corresponds roughly to that in the center of a proton. At the phase transition, the normalized energy density e/T^4 rises rapidly by about an order of magnitude over a narrow temperature interval $\Delta T \lesssim 15 - 20\,{\rm MeV}$, whereas the pressure p/T^4 (which is proportional to the grand canonical thermodynamic potential) is continuous and rises more gradually (Fig. 1). Both seem to saturate at about 80-85% of the Stefan-Boltzmann value for an ideal gas of noninteracting quarks and gluons, the energy density more quickly (at about $1.2\,T_{\rm cr}$), the pressure more slowly. Above about $2\,T_{\rm cr}$, the lattice data follow the Equation of State of an ideal gas of massless particles, $e = 3p$.

For many years this observation has been interpreted as lattice QCD support for the hypothesis of a weakly interacting, perturbative QGP. The recent RHIC data taught us (as I will show) that this interpretation was quite wrong.

It was recognized over 3 decades ago (see review [2]) that information about the EOS of

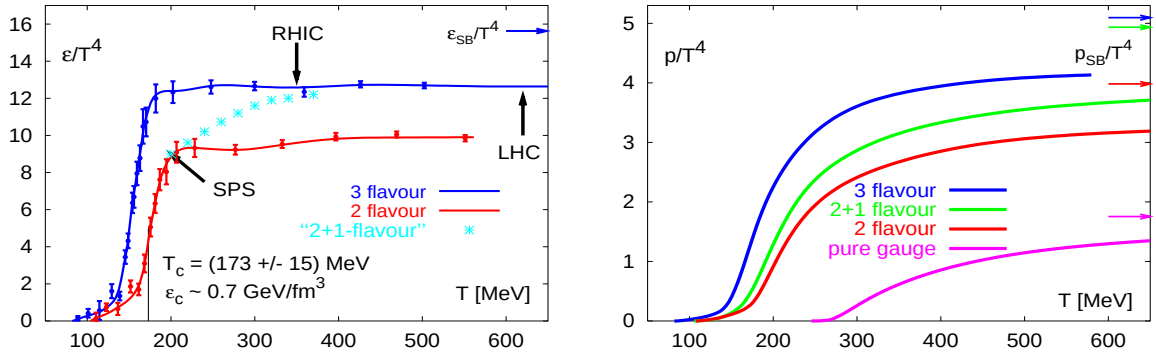

Figure 1. The normalized energy density e/T^4 (left) and pressure p/T^4 (right) from lattice QCD [1] for 0, 2 and 3 light quark flavors, as well as for 2 light + 1 heavier (strange) quark flavors. Horizontal arrows on the right indicate the corresponding Stefan-Boltzmann values for a non-interacting quark-gluon gas.

[1] Email: heinz.9@osu.edu. Work supported by the U.S. Department of Energy, grant DE-FG02-01ER41190.

strongly interacting matter can be extracted by studying the collective dynamics of relativistic heavy-ion collisions. This connection is particularly direct in the framework of *ideal fluid dynamics* which becomes applicable if the matter formed in the collision approaches *local thermal equilibrium*. The latter requires sufficiently strong interactions in the medium that local relaxation time scales are shorter than the macroscopic evolution time scale. In this limit the local conservation laws for the baryon number, energy and momentum currents, $\partial_\mu j_B^\mu(x) = 0$ and $\partial_\mu T^{\mu\nu} = 0$, can be rewritten as the relativistc Euler equations for ideal fluid motion:

$$\dot{n}_B = -n_B\,(\partial\cdot u), \qquad \dot{e} = -(e+p)\,(\partial\cdot u), \tag{1}$$

$$\dot{u}^\mu = \frac{\nabla^\mu p}{e+p} = \frac{c_s^2}{1+c_s^2}\,\nabla^\mu \ln\left(\frac{e}{e_0}\right). \tag{2}$$

The dot denotes the time derivative in the local fluid rest frame ($\dot{f} = u\cdot\partial f$) and ∇^μ the gradient in the directions tranverse to the fluid 4-velocity u^μ. The first line describes the dilution of baryon and energy density due to the local expansion rate $\partial\cdot u$, which itself is driven according to (2) by the pressure or energy density gradients providing the fluid acceleration. The absolute value of the energy density e is locally irrelevant: the initial maximal energy density e_0 only matters by setting the overall time scale between the beginning of hydrodynamic expansion and final decoupling, thereby controlling how much flow can develop globally. The details of the flow pattern are thus entirely controlled by the temperature dependent speed of sound $c_s^2 = \frac{\partial p}{\partial e}$.

According to the LQCD data, the latter is $c_s^2 \approx \frac{1}{3}$ for $T > 2\,T_{\rm cr}$, then drops steeply near $T \approx T_{\rm cr}$ to values near $c_s^2 \approx \frac{1}{20}$ (the "softest point", see Fig. 11 in [1]), before rising again in the hadron resonance gas phase to $c_s^2 \approx 0.15$ [3]. A key goal of flow studies in relativistic heavy ion collisions is to find traces of this "softest point" in the data.

2. "Flavors" of transverse flow in heavy ion collisions

Experimentally one studies flow by analyzing the transverse momentum spectra of the emitted hadrons. In central ($b = 0$) collisions between spherical nuclei, the flow is azimuthally symmetric about the beam axis. This "radial flow" integrates over the entire pressure history of the collision from initial thermalization to final decoupling ("freeze-out"), due to persistent pressure gradients. In noncentral ($b \neq 0$) collisions, or central collisions between deformed nuclei such as uranium [4], the nuclear reaction zone is spatially deformed, and anisotropies of the transverse pressure gradients result in transverse flow anisotropies. These can be quantified by Fourier expanding the measured final momentum spectrum $dN/(dy\,p_\perp dp_\perp\,d\phi_p)$ with respect to the azimuthal angle ϕ_p. For collisions between equal nuclei, the first non-vanishing Fourier coefficient at midrapidity is the *elliptic flow* $v_2(p_\perp, b)$. Since v_2 is driven by pressure *anisotropies* and the spatial deformation of the reaction zone creating such anisotropies quickly decreases as time proceeds, the elliptic flow is sensitive to the EOS only during the early expansion stage [5] (the first $\sim 5\,{\rm fm}/c$ in semicentral Au+Au collisions [6]), until the spatial deformation has disappeared.

Depending on the initial energy density (i.e. beam energy), the hot expanding fireball spends this crucial time either entirely in the QGP phase, or mostly near the quark-hadron phase transition, or predominantly in the hadron resonance gas phase [6], thereby probing different effective values of the sound speed c_s. To the extent that ideal fluid dynamics is valid in all these cases, an excitation function of the elliptic flow v_2 should thus allow to map the temperature dependence of the speed of sound and identify the quark-hadron phase transition, via a minimum in the function $v_2(\sqrt{s})$ [6]. This will be further discussed below (see Section 5.2 and Fig. 6).

3. Model parameters and predictive power of hydrodynamics

The hydrodynamic model requires *initial conditions* at the earliest time at which the assumption of local thermal equilibrium is applicable, and a *"freeze-out prescription"* at the end when the system becomes too dilute to maintain local thermal equilibrium. Both are described in

detail elsewhere [7]. Different approaches to freeze-out invoke either the Cooper-Frye algorithm [8] (used by us), in which chemical freeze-out of the hadron abundances at $T_{\rm cr}$ [9] must be implemented by hand by introducing non-equilibrium chemical potentials below $T_{\rm cr}$ [10, 11, 12], or a hybrid approach [13, 14] that switches from a hydrodynamic description to a microscopic hadron cascade at the quark-hadron transition, letting the cascade handle the chemical and thermal freeze-out kinetics. While the radial flow patterns from the two freeze-out procedures don't differ much, the elliptic flow can be quite different if the spatial deformation of the fireball is still significant during the hadronic stage of the expansion, as I will discuss in Sec. 5.2.

We have solved the relativistic equations for ideal hydrodynamics under the simplifying assumption of boost-invariant longitudinal expansion (see [6, 15] for details). This is adequate near midrapidity (the region which most RHIC experiments cover best), but not sufficient to describe the rapidity distribution of emitted hadrons and of their transverse flow pattern which require a (3+1)-dimensional hydrodynamic code such as the one by Hirano [10].

The initial and final conditions for the hydrodynamic evolution are fixed by fitting the pion and proton spectra at midrapidity in *central* ($b=0$) collisions; additionally, we use the centrality dependence of the total charged multiplicity $dN_{\rm ch}/dy$. I stress that this is the *only* information used from $b\neq 0$ collisions, and it is necessary to fix the ratio of soft to hard collision processes in the initial entropy production. An upper limit for the initial thermalization time $\tau_0 \leq 0.6\,{\rm fm}/c$, the initial entropy density $s_0 = 110\,{\rm fm}^{-3}$ in the fireball center (corresponding to an initial maximal energy density $e_0 \approx 30\,{\rm GeV/fm}^3$ and an initial central fireball temperature $T_0 \approx 360\,{\rm MeV} \approx 2\,T_{\rm cr}$), the baryon to entropy ratio, and the freeze-out energy density $e_{\rm dec} = 0.075\,{\rm GeV/fm}^3$ are all fixed from the $b=0$ pion and proton spectra (these numbers refer to 200 A GeV Au+Au collisions at RHIC [12]). The initial entropy density profile is calculated for all b from the collision geometry, using the Glauber model with soft/hard ratio as fixed above. Except for pions and protons, all other hadron spectra in $b=0$ collisions and all spectra for $b\neq 0$ collisions (including all flow anisotropies such as v_2 which vanish at $b=0$) are then parameter-free predictions of the model. Note that all calculated hadron spectra include feeddown from decays of unstable hadron resonances.

4. Successes of ideal fluid dynamics at RHIC

4.1. Hadron momentum spectra and radial flow

Figure 2 shows the single particle $p_\perp$-spectra for pions, kaons and antiprotons (left panel) as well as Ω baryons (right panel) measured in Au+Au collisions at RHIC, together with hydrodynamical results [12]. In order to illustrate the effect of additional radial flow generated in the late hadronic stage below $T_{\rm cr}$, two sets of curves are shown: the lower (blue) bands correspond to kinetic decoupling at $T_{\rm cr} = 165\,{\rm MeV}$, whereas the upper (red) bands assume decoupling at $T_{\rm dec} = 100\,{\rm MeV}$. The width of the bands indicates the sensitivity of the calculated spectra to

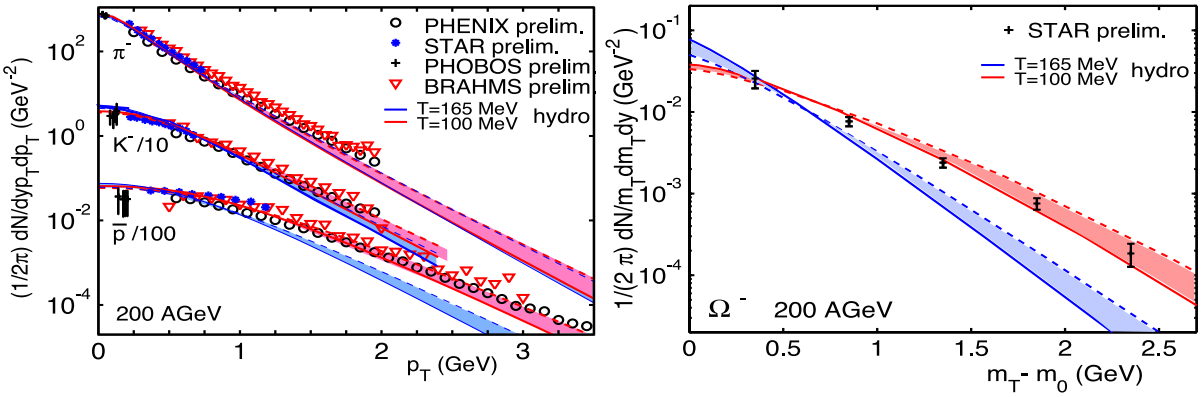

Figure 2. Negative pion, kaon, antiproton, and Ω spectra from central Au+Au collisions at $\sqrt{s} = 200\,A\,{\rm GeV}$ measured at RHIC [16]. The curves show hydrodynamical calculations [12] (see text).

an initial transverse flow of the fireball already at the time of thermalization [12]. In the hydrodynamic simulation it takes about 9-10 fm/c until most of the fireball becomes sufficiently dilute to convert to hadronic matter and another 7-8 fm/c to fully decouple [6]. Figure 2 shows that by the time of hadronization the dynamics has not yet generated enough radial flow to reproduce the measured $\bar{p}$ and Ω spectra; these heavy hadrons, which are particularly sensitive to radial flow, require the additional collective "push" created by resonant quasi-elastic interactions during the fairly long-lived hadronic rescattering stage. The flattening of the $\bar{p}$ spectra by radial flow provides a natural explanation for the (initially puzzling) experimental observation that for $p_\perp > 2\,\mathrm{GeV}/c$ antiprotons become more abundant than pions [15].

As shown elsewhere (see Fig. 1 in [17]), the model describes these and all other hadron spectra not only in central, but also in *peripheral* collisions, up to impact parameters of about 10 fm, and with similar quality. No additional parameters enter at non-zero impact parameter.

4.2. Elliptic flow

Figure 3 shows the predictions for the elliptic flow coefficient v_2 from Au+Au collisions at RHIC, together with the data [18, 19]. For impact parameters $b \leq 7$ fm ($n_{\mathrm{ch}}/n_{\mathrm{max}} \geq 0.5$) and transverse

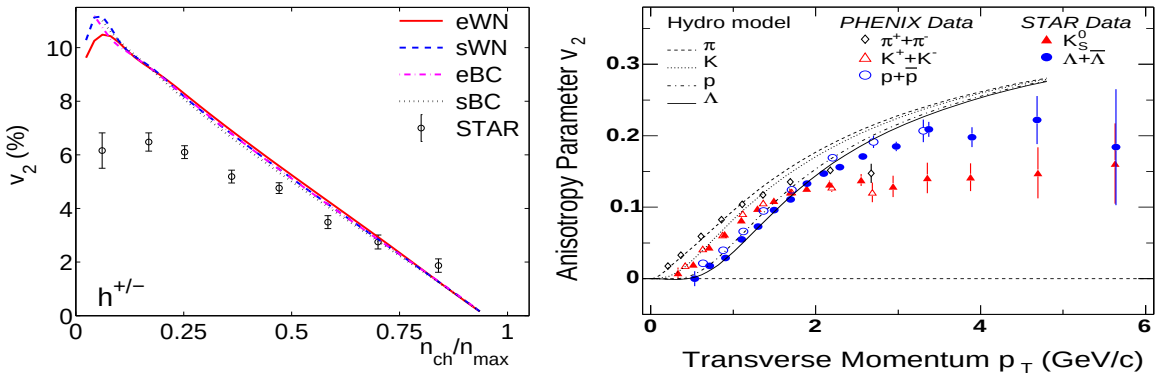

Figure 3. Left: $p_\perp$-averaged elliptic flow for all charged hadrons from 130 A GeV Au+Au collisions, as a function of collision centrality (n_{ch} is the charged multiplicity at $y = 0$). The curves are hydrodynamic calculations with different choices for the initial energy density profile (see [20]). Right: Differential elliptic flow $v_2(p_\perp)$ for identified hadrons from minimum bias Au+Au collisions at 200 A GeV [18, 19, 21], together with hydrodynamic curves from [22].

momenta $p_\perp \lesssim 1.5\,\mathrm{GeV}/c$ the data are seen (left panel of Fig. 3) to exhaust the upper limit for v_2 obtained from the hydrodynamic calculations. For larger impact parameters $b > 7$ fm the $p_\perp$-averaged elliptic flow v_2 increasingly lags behind the hydrodynamic prediction; this will be discussed in detail in Sec. 5.2. As a function of $p_\perp$ (right panel of Fig. 3) the elliptic flow of all hadrons measured so far is very well described by hydrodynamics, for $p_\perp \lesssim 1.5 - 2\,\mathrm{GeV}/c$. In particular the hydrodynamically predicted *mass splitting* of v_2 at low $p_\perp$ is perfectly reproduced by the data. This mass splitting depends on the EOS [22], and the EOS including a quark-hadron phase transition used here describes the data better than one without phase transition (see Fig. 2 in [17]). Ideal fluid dynamics with a QGP EOS thus gives an excellent and very detailed description of *all* hadron spectra below $p_\perp = 1.5\,\mathrm{GeV}/c$. Since this $p_\perp$-range includes more than 99% of all produced hadrons, it is fair to say that *the bulk of the fireball matter formed in Au+Au collisions at RHIC behaves very much like a perfect fluid.*

4.3. Final source eccentricity in coordinate space

While spectra and elliptic flow reflect the *momentum* structure of the hadron emitting source, its *spatial* deformation can be tested with 2-pion Hanbury Brown-Twiss (HBT) correlations measured as a function of the azimuthal emission angle [23, 24]. Even though the initial spatial

deformation of the reaction zone in non-central Au+Au collisions at RHIC is finally completely gone, many pions are already emitted from earlier times when the spatial deformation is still significant. For Au+Au collisions at $b = 7$ fm, the spatial eccentricity of the time-integrated hydrodynamic pion emission function is $\langle \varepsilon_x \rangle = 0.14$ (or 56% of its initial value $\varepsilon_x(\tau_0) = 0.25$) [23]. Using azimuthally sensitive pion HBT measurements, the STAR Collaboration has measured in the corresponding impact parameter bin [25] $\langle \varepsilon_x \rangle = 0.11 \pm 0.035$ (or $45 \pm 15\%$ of the initial deformation). This agreement can be counted as another success for the hydrodynamic model.

5. Viscous effects at RHIC

5.1. QGP viscosity

As evident in the right panel of Fig. 3, the hydrodynamic prediction for $v_2(p_\perp)$ gradually breaks down above $p_\perp \gtrsim 1.5\,\mathrm{GeV}/c$ for mesons and above $p_\perp \gtrsim 2.2\,\mathrm{GeV}/c$ for baryons. The empirical fact [21] that both the $p_\perp$-values, where this break from hydrodynamics sets in, and the saturation values for v_2 at high $p_\perp$ for baryons and mesons are always (*i.e. for all collision centralities!*) related by 3 : 2 (i.e. by their ratios of valence quark numbers), independent of their masses, tells its own interesting story (see e.g. [26]): It strongly suggests that in this $p_\perp$ region hadrons are formed by coalescence of color-deconfined quarks, and that the elliptic flow is of partonic origin (i.e. generated before hadronization), with a $p_\perp$-shape that follows hydrodynamics at low $p_\perp$ up to about 750 MeV and then gradually breaks away [26].

Since $v_2(p_\perp)$ is a measure for the relatively small differences between the in-plane and out-of-plane slopes of the $p_\perp$ spectra, it is more sensitive to deviations from ideal fluid dynamic behaviour than the angle-averaged slopes. Two model studies [27, 28] showed that v_2 reacts particularly strongly to shear viscosity. As the mean free path of the plasma constituents (and thus the fluid's viscosity) goes to zero, v_2 approaches the ideal fluid limit from below [29] (see Fig. 4a). At higher transverse momenta it does so more slowly than at low $p_\perp$ [29], approaching a constant saturation value at high $p_\perp$. The increasing deviation from the ideal fluid limit for

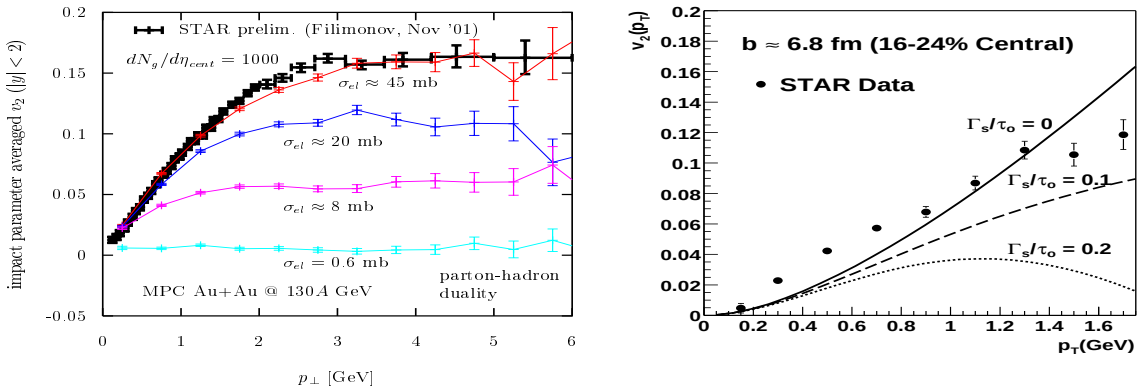

Figure 4. Left: Elliptic flow from a parton cascade [29], compared with STAR data, for different parton-parton scattering cross sections. Larger cross sections lead to smaller mean free paths. Right: Perturbative effects of shear viscosity on the elliptic flow $v_2(p_\perp)$ [28] (see text).

growing $p_\perp$ is qualitatively consistent with the expected influence of shear viscosity: Teaney [28] showed that the lowest order viscous corrections to the local equilibrium distribution increase quadratically with $p_\perp$ so that v_2 remains increasingly below the ideal fluid limit as $p_\perp$ grows (see Fig. 3b). From Fig. 4b Teaney concluded that at RHIC the normalized sound attenuation length $\frac{\Gamma_s}{\tau} = \frac{4}{3T\tau}\frac{\eta}{s}$ (where η is the shear viscosity, T the temperature and s the entropy density) cannot be much larger than about 0.1. This puts a stringent limit on the dimensionless ratio η/s, bringing it close to the recently conjectured absolute lower limit for the viscosity of $\eta/s = \hbar/(4\pi)$ [30]. This would make the quark-gluon plasma the most ideal fluid ever observed [30].

These arguments show that deviations from ideal fluid dynamics at high $p_\perp$ must be expected, and that they can be large even for fluids with very low viscosity. At which $p_\perp$ non-ideal

effects begin to become visible in $v_2(p_\perp)$ can be taken as a measure for the fluid's viscosity. To answer the *quantitative* question what the RHIC data on partonic elliptic flow and its increasing deviation from ideal fluid behaviour above $p_\perp \gtrsim 750\,\mathrm{MeV}/c$ imply for the *value* of the QGP shear viscosity η requires a numerical algorithm for solving viscous relativistic hydrodynamics (see [31] for an update).

5.2. Viscosity of the hadron resonance gas

Ideal fluid dynamics also fails to describe the elliptic flow v_2 in more peripheral Au+Au collisions at RHIC and in central and peripheral collisions at lower energies (see Fig. 5a), as well as at forward rapidities in minimum bias Au+Au collisions at RHIC [32]. Whereas hydrodynamics predicts a non-monotonic beam energy dependence of v_2 (Fig. 6a [6]), with largest values at upper AGS and lower SPS energies, somewhat lower values at RHIC and again larger values at the LHC, the data seem to increase monotonically with $\sqrt{s}$.

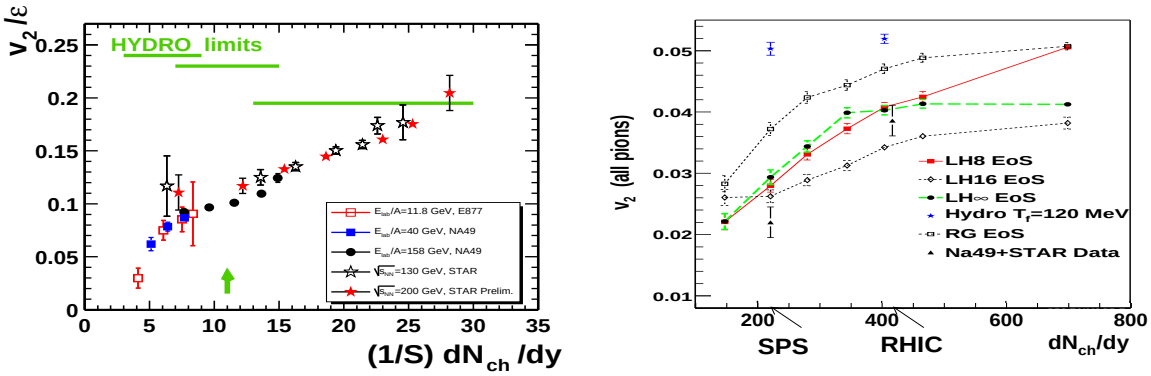

Figure 5. Left: Scaled elliptic flow v_2/ε (where ε denotes the initial spatial eccentricity) vs. the charged multiplicity density per unit initial transverse overlap area S [33]. Right: Elliptic flow v_2 for minimum bias Au+Au collisions at various collision energies, parametrized by the final charged multiplicity density at midrapidity [14]. See text for discussion.

Such a monotonic rise is consistent with "hybrid" calculations by Teaney [14] (Fig. 5b) where the fireball undergoes ideal fluid dynamic evolution only while in the QGP, followed by hadronic *kinetic* evolution using RQMD after hadronization. Figure 5b shows several curves corresponding to different equations of state during the hydrodynamic evolution (see [14]), with LH8 being closest to the data. The difference between the points labelled LH8 and the hydrodynamic values at the top of the figure is due to the different evolution during the late hadronic stage. Obviously, at lower collision energies and for impact parameters $b \sim 7\,\mathrm{fm}$ (which dominate v_2 in minimum bias collisions), ideal fluid dynamics continues to build additional elliptic flow during the hadronic stage, but RQMD does not. The initial energy densities are smaller than at RHIC and the fireball does not spend enough time in the QGP phase for the spatial eccentricity ε to fully disappear before entering the hadron resonance gas phase. Anisotropic pressure gradients thus still exist in the hadronic phase, and ideal fluid dynamics reacts to them according to the stiffness of the hadron resonance gas EOS ($p \approx 0.15e$). Teaney's calculations [14] show that RQMD responds to these remaining anisotropies much more weakly, building very little if any additional elliptic flow during the hadronic phase. The hadron resonance gas is a highly viscous medium, unable to maintain local thermal equilibrium. The failure of the hydrodynamic model in situations where the initial energy density is less than about $10\,\mathrm{GeV/fm}^3$ [34] is therefore likely *not* the result of viscous effects in the early QGP fluid, but rather caused by the highly viscous late hadronic stage which is unable to efficiently respond to any remaining spatial fireball eccentricity. Similar arguments hold at forward rapidities at RHIC [34] where the initial energy densities are also significantly smaller than at midrapidity while the initial spatial eccentricities are similar.

The large hadron gas viscosity spoils one of the clearest experimental signatures for the quark-hadron phase transition, the predicted [6] non-monotonic beam energy dependence of v_2 which was already described in Sec. 2 and is shown in Fig. 6a. As one comes down from infinite beam energy, v_2 is predicted to first decrease (due to the softening of the EOS in the phase transition region) and then recover somewhat in the moderately stiff hadron gas phase. The hadron gas viscosity spoils this recovery, leading to an apparently monotonous decrease of v_2 with falling beam energy (Fig. 5). However, recent PHENIX data from Au+Au collisions at $\sqrt{s} = 62\,A\,\mathrm{GeV}$ [35] indicate that this decrease may not be quite as monotonous as suggested by Fig. 5a. Figure 6b shows that, at fixed $p_\perp$, the elliptic flow $v_2(p_\perp)$ is essentially constant over the entire energy range explored at RHIC (from 62 to 200 A GeV), decreasing only when going further down to SPS and AGS energies. When integrated over $p_\perp$, this turns into a monotonous behaviour as in Fig. 5a, due to the steepening $p_\perp$ spectra at lower $\sqrt{s}$. While Fig. 6b does not confirm the hydrodynamically predicted *rise* of v_2 towards lower $\sqrt{s}$, it may still reflect this predicted non-monotonic structure in the elliptic flow excitation function, after strong dilution by hadronic viscosity effects. Obviously, many and more systematic hybrid calculations of the type pioneered by Teaney [14] are necessary to explore to what extent we can eventually prove the existence of a QCD phase transition using elliptic flow data in the SPS-RHIC energy domain.

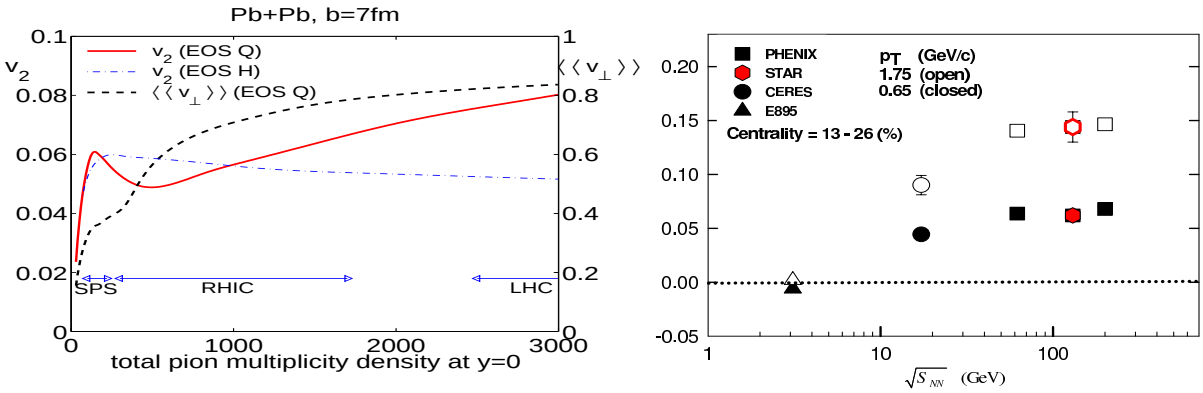

Figure 6. Left: Excitation function of radial and $p_\perp$-integrated elliptic flow for $b = 7$ fm Pb+Pb or Au+Au collisions [6]. The horizontal axis gives $dN_\pi/dy(b{=}7\,\mathrm{fm})$, and the horizontal arrows indicate how dN_π/dy was expected to correspond to the beam energy ranges covered by SPS, RHIC and LHC before the RHIC data were available. Right: Elliptic flow at fixed $p_\perp = 0.65$ and 1.75 GeV/c from A+A collisions with $A \approx 200$ at a variety of beam energies [35].

Obviously, it will be important to confirm non-viscous fluid behaviour at higher initial energy densities than so far explored, by extending Fig. 5a to the right and verifying that v_2/ε settles on the hydrodynamic curve. This can be done with Pb+Pb collisions at the LHC, or with full-overlap U+U collisions at RHIC [4]. In addition, the large spatial source deformations achievable in full-overlap side-on-side U+U collisions allow for decisive systematic studies of the non-linear path-length dependence of QCD radiative energy loss of fast partons. In [4] we give quantitative arguments why a U+U collision program should be seriously considered at RHIC.

6. Conclusions

The collective flow patterns observed at RHIC provide strong evidence for fast thermalization at less than 1 fm/c after impact and at energy densities more than an order of magnitude above the critical value for color deconfinement. The thus created thermalized QGP is a strongly coupled plasma which behaves like an almost ideal fluid. These features are first brought out in heavy-ion collisions at RHIC because only there the initial energy densities and QGP life times are large enough for the ideal fluid character of the QGP to really manifest itself, in the form of fully saturated hydrodynamic elliptic flow, undiluted by late non-equilibrium effects from the highly viscous hadron resonance gas which dominates the expansion at lower energies.

We are now ready for a systematic experimental and theoretical program to quantitatively extract the EOS, thermalization time and transport properties of QGP and hot hadronic matter. This requires more statistics and a wider systematic range for soft hadron production data, but more importantly a wide range of systematic simulation studies with the "hydro-hadro" hybrid algorithms and, above all, a (3+1)-dimensional viscous relativistic hydrodynamic code (see [31] for more on that).

References

[1] Karsch F and Laermann E 2004 *Quark-Gluon Plasma 3*, ed R C Hwa and X-N Wang (Singapore: World Scientific) p 1
[2] Stöcker H and Greiner W 1986 *Phys. Rept.* **137** 277
[3] Sollfrank J *et al* 1997 *Phys. Rev.* C **55** 392
[4] Heinz U and Kuhlman A 2005 *Phys. Rev. Lett.* **94**, in press (*Preprint* nucl-th/0411054)
[5] Sorge H 1997 *Phys. Rev. Lett.* **78** 2309
[6] Kolb P F, Sollfrank J, and Heinz U 2000 *Phys. Rev.* C **62** 054909.
[7] Heinz U 2004 *AIP Conf. Proc.* **739** 163
[8] Cooper F and Frye G 1974 *Phys. Rev.* D **10** 186
[9] Braun-Munzinger P, Magestro D, Redlich K, and Stachel J 2001 *Phys. Lett.* B **518** 41
[10] Hirano T and Tsuda K 2002 *Phys. Rev.* C **66** 054905
[11] Rapp R 2002 *Phys. Rev.* C **66** 017901; Teaney D 2002 *Preprint* nucl-th/0204023
[12] Kolb P F and Rapp R 2003 *Phys. Rev.* C **67** 044903
[13] Bass S A and Dumitru A 2000 *Phys. Rev.* C **61** 064909
[14] Teaney D, Lauret J, and Shuryak E V 2001 *Phys. Rev. Lett.* **86** 4783 and *Preprint* nucl-th/0110037
[15] Kolb P F and Heinz U 2004 *Quark-Gluon Plasma 3*, ed R C Hwa and X-N Wang (Singapore: World Scientific) p 634
[16] PHENIX Collaboration, Chujo T *et al* 2003 *Nucl. Phys.* **A715** 151c;
STAR Collaboration, Barannikova O, Wang F *et al* 2003 *Nucl. Phys.* **A715** 458c;
PHOBOS Collaboration, Wosiek B *et al* 2003 *Nucl. Phys.* **A715** 510c;
BRAHMS Collaboration, Ouerdane D *et al* 2003 *Nucl. Phys.* **A715** 478c;
STAR Collaboration, Suire C *et al* 2003 *Nucl. Phys.* **A715** 470c
[17] Heinz U and Kolb P F 2002 *Proc. 18th Winter Workshop on Nuclear Dynamics*, ed. R. Bellwied, J. Harris, and W. Bauer (Debrecen, Hungary: EP Systema) p.205 (*Preprint* hep-ph/0204061)
[18] STAR Collaboration, Ackermann K H *et al* 2001 *Phys. Rev. Lett.* **86** 402;
STAR Collaboration, Adler C *et al* 2001 *Phys. Rev. Lett.* **87** 182301;
STAR Collaboration, Adler C *et al* 2002 *Phys. Rev. Lett.* **89** 132301 and *Phys. Rev.* C **66** 034904;
STAR Collaboration, Adler C *et al* 2003 *Phys. Rev. Lett.* **90** 032301;
STAR Collaboration, Adams J *et al* 2004 *Phys. Rev. Lett.* **92** 052302
[19] PHENIX Collaboration, Adcox K *et al* 2002 *Phys. Rev. Lett.* **89** 212301;
PHENIX Collaboration, Adler S S *et al* 2003 *Phys. Rev. Lett.* **91** 182301
[20] Kolb P F, Heinz U, Huovinen P, Eskola K J, and Tuominen K 2001 *Nucl. Phys.* **A696** 175
[21] Sorensen P R 2003 Kaon and Lambda production at intermediate p(T): Insights into the hadronization of the bulk partonic matter created in Au + Au collisions at RHIC, Ph.D. thesis (*Preprint* nucl-ex/0309003)
[22] Huovinen P, Kolb P F, Heinz U, Ruuskanen P V and Voloshin S A 2001 *Phys. Lett* B **503** 58
[23] Heinz U and Kolb P 2002 *Phys. Lett.* B **542** 216
[24] Retière F and Lisa M A 2004 *Phys. Rev.* C **70** 044907
[25] STAR Collaboration, Adams J *et al* 2004 *Phys. Rev. Lett.* **93** 012301
[26] Müller B 2005 *Nucl. Phys.* **A750** 84; Molnar D and Voloshin S A 2003 *Phys. Rev. Lett.* **91** 092301
[27] Heinz U and Wong S M H 2002 *Phys. Rev.* C **66** 014907
[28] Teaney D 2003 *Phys. Rev.* C **68** 034913 and private communication
[29] Molnar D and Gyulassy M 2002 *Nucl. Phys.* **A697** 495 (Erratum *ibid.* **A703** 893);
[30] Kovtun P, Son D T, and Starinets A O 2004 *Preprint* hep-th/0405231
[31] Chaudhuri A K and Heinz U 2005 these proceedings
[32] Hirano T 2002 *Phys. Rev.* C **65** 011901
[33] NA49 Collaboration, Alt C *et al* 2003 *Phys. Rev.* C **68** 034903
[34] Heinz U and Kolb P F 2004 *J. Phys. G: Nucl. Phys.* **30** S1229
[35] PHENIX Collaboration, Adler S S *et al* 2004 *Preprint* nucl-ex/0411040